Sustained Spatiotemporal Patterns in the Bromate−Sulfite Reaction

Zsanett Virányi,[†] István Szalai,[‡] Jacques Boissonade,[§] and Patrick De Kepper*[,§]

Department of Physical Chemistry, University of Szeged, P.O. Box 105, H-6701 Szeged, Hungary, Institute of Chemistry, L. Eötvös University, P.O. Box 32, H-1518 Budapest 112, Hungary, and Centre de Recherche Paul Pascal, Centre National de la Recherche Scientifique Bordeaux, Avenue Schweitzer, F-33600 Pessac, France

Received: March 26, 2007; In Final Form: May 24, 2007

The acid autoactivated bromate−sulfite reaction exhibits spatial bistability, travelling acid−base fronts, and spatiotemporal oscillations when operated in an unstirred one-side-fed spatial reactor. We show that a skeleton kinetic model, recently proposed by Szántó and Rábai, in which we take into account the charge and the actual diffusivity of solvated ions, provides theoretical results in good agreement with experimental observations. The differences with previous observations made with the homologous iodate−sulfite reaction are discussed. Despite the analogies in the phase diagram of these two systems, it is concluded that the relevant kinetic mechanism of the iodate−sulfite system cannot be just a homologous transcription of that presently working well for the bromate−sulfite system, even in excess sulfite conditions.

Introduction

The study of pattern formation in chemical reaction−diffusion systems is one of the challenging fields of nonlinear dynamics.[1−4] Although quite a large variety of spatiotemporal behaviors have been observed in the past decades,[2−4] such as excitability or phase waves, and standing Turing and front patterns, these patterns have been produced in only a handful of reactions. Besides the Belousov−Zhabotinsky, the chlorite−iodide−malonic−acid, and the iodate−sulfite−ferrocyanide reactions,[2] sustained spatiotemporal patterns were recently observed with the chlorite−tethrationate (CT)[5,6] and iodate−sulfite (IS)[7] reactions in continuously fed spatial reactors. In continuous stirred tank reactors (CSTRs), tens of reaction families, amounting to hundreds of variants, are known to produce temporal self-organization phenomena such as bistability and oscillations.[3] These phenomena depend on autoactivatory kinetic processes eventually quenched by competing inhibitory processes. Such kinetic mechanisms are appropriate for the development of reaction−diffusion patterns in unstirred systems. Although the general theoretical conditions for the development of reaction−diffusion patterns are well-established,[3,8] the effective control of their development in significantly different real chemical systems is still poorly documented.[9] It is thus important to explore chemically different systems to distinguish the general aspects from the specificities of each case.

In this vein, we have recently studied the dynamics of the acid autocatalytic CT and IS reactions in one-side-fed spatial reactors (OSFRs). Although these reactions only exhibit temporal bistability in a CSTR, they both give rise to sustained spatiotemporal oscillations and traveling excitability waves, in addition to the naturally expected spatial bistability[5−7] in an OSFR. Spatial bistability is a direct extension of the CSTR bistability to spatial systems. In an OSFR, the fresh reactants fed into the CSTR and the chemicals produced therein diffuse into a porous medium. This porous part, often made of a hydrogel, is the actual place where the chemical concentration patterns resulting from the sole interplay between reaction and diffusion develop. Spatial bistability corresponds to the coexistence of two different stable concentration profiles in the gel for the same fixed boundary composition (i.e., same state of the CSTR).[10,11] The spatial states preserve the symmetry imposed by the feed at the boundary. It was shown in spatially bistable systems that, when the activatory species diffuses faster than the inhibitory species, oscillatory and excitability phenomena may emerge even when the homogeneous kinetic mechanism has no oscillatory capability. This can naturally occur in acid-autocatalytic reactions where the proton diffuses much faster than the other species.[6,11]

Here, we present a systematic study of the spatiotemporal dynamics of the bromate−sulfite (BS) reaction in an OSFR. The BS reaction is a typical clock reaction: in the concentration range considered in this report, an unbuffered mixture, initially at pH = 7, undergoes a slow decrease of the pH that eventually, suddenly drops to pH ≈ 2 after a well-defined induction time. When this reaction is operated in a CSTR, Edblom et al.[12] have shown that the reaction system gives rise to steady-state bistability. More recently, Szanto and Rabai[13] have also shown that at very long residence times (i.e., 5×10^3 s) large amplitude pH oscillations could be observed, in addition to bistability. These authors show that the above experimental facts are well accounted for when, following old kinetic and stoichiometric works,[14,15] it is considered that the oxidation of sulfite proceeds through competing two- and one-electron-transfer channels. These competing channels can be globally represented by the following mass balance equations:

$$BrO_3^- + 3HSO_3^- \rightarrow 3SO_4^{2-} + Br^- + 3H^+ \quad (R1)$$

$$BrO_3^- + 6HSO_3^- \rightarrow 3S_2O_6^{2-} + Br^- + 3H_2O \quad (R2)$$

The positive feedback is generated by an autoactivated production of protons through channel R1, where sulfite ions are oxidized to sulfate ions. Conversely, the R2 reaction channel, associated with the fast protonation equilibrium of sulfite ions

* To whom correspondence should be addressed. E-mail: dekepper@crpp-bordeaux.cnrs.fr.
[†] University of Szeged.
[‡] L. Eötvös University.
[§] Centre de Recherche Paul Pascal.

10.1021/jp0723721 CCC: $37.00
Published on Web 08/02/2007

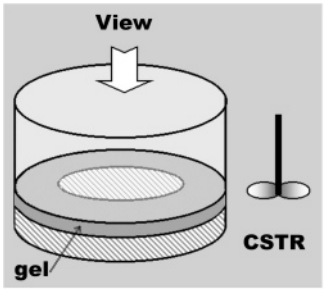

Figure 1. Schematic diagram of the annular unstirred OSFR. The gel annulus exchanges chemicals with the contents of the CSTR by the external rim only, the viewing direction is orthogonal to the feed direction of the gel part.

(see model in 1), is a proton consuming process that leads to the formation of relatively stable dithionate ions. This channel provides an appropriate negative feedback for the emergence of temporal oscillations in a CSTR.

In an OSFR, the homologous IS reaction that shows no oscillatory behavior in a CSTR exhibits spatiotemporal oscillations and excitability. The mechanism at the origin of this dynamical behavior is not yet established. These may come from a differential diffusion mechanism,[7] as in the CT reaction, but more recent observations challenge this interpretation. These dynamical instabilities could be promoted by some underlying oscillatory kinetic mechanism.[16]

Beside providing a new example of a chemical system capable of developing spatiotemporal reaction−diffusion patterns, the present study gives the possibility of comparing the OSFR dynamics of two homologous BS and IS reactions. The significant chemical kinetic pathways seem to be well identified in the BS reaction. Actually, we shall show that the model proposed by Rábai and co-workers for the BS reaction leads to numerical results in semiquantitative agreement with both the CSTR and the OSFR experimental observations. On the contrary, the modeling of the IS reaction is still deficient.[16]

Experimental Section

The core of our OSFR consists of a flat annular piece of gel tightly inserted into a circular rectangular groove left between an upper polished transparent Plexiglas cylinder and a lower cylinder made of Teflon (see Figure 1). This gel holder is immersed into the contents of the CSTR. The gel annulus, made of a 2% agarose (Fluka 05070) network, has an outer radius $r = 25$ mm, a width (the difference between the external and internal radius) $w = 1.0$ or 2.0 mm, and a height (or thickness) $h = 0.25$ mm. Only the outer rim of the annulus is in contact with the contents of the CSTR. This design makes it possible to observe the color changes across the width of the flat annulus (Figure 1). The volume of the CSTR is $V = 25$ cm^3. The residence time $\tau = 500$ s and the CSTR bath temperature $T = 30$ °C were kept constant. The feed is provided by three separate streams of chemicals, injected by precision pumps (Pharmacia P 500), which enter the CSTR by a single inlet port. The first stream contains a fixed concentration of a sodium sulfite ($[Na_2SO_3]_0 = 60$ mM; Aldrich) solution. The second and the third streams contain variable concentrations of sodium bromate ($[NaBrO_3]_0$ ranging from 0 to 220 mM; Prolabo) and sulfuric acid ($[H_2SO_4]_0$ ranging from 0 to 16.7 mM; Fluka) solutions. The bracketed terms $[X]_0$ are the concentration that species X would have in a collective feed-stream prior to any reaction. The solutions contain bromophenol blue, a pH color indicator that changes from purple-blue (basic) to yellow-orange (acidic) around pH = 3.8, which appear as dark and light gray, respectively, in the pictures presented in this report. In this study, all reactants are reagent-grade chemicals used without further purification. Solutions were prepared daily in deionized water. The sulfite solution was maintained under a nitrogen atmosphere to prevent air oxidation. The chemical state of the CSTR is monitored by the redox potential of a bright platinum electrode. A pH electrode at the outlet port measures the pH of the CSTR solution. The color profiles of stationary states and the wave patterns in the gel are monitored by a CCD camera, and the dynamics are recorded on a time-lapse VCR. A frame grabber digitizes the images for further processing.

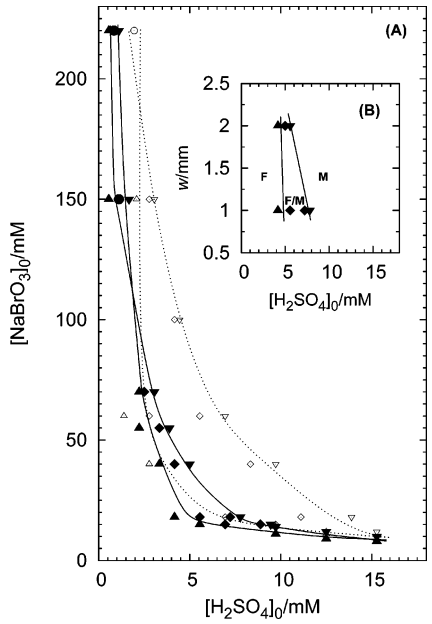

Figure 2. (A) Experimental nonequilibrium phase diagram in the ($[BrO_3^-]_0$, $[H_2SO_4]_0$) plane at $w = 1$ mm. The symbols correspond the experimental points. The full symbols are attributed to the states of the gel: ▼ stable M state; ▲ stable F state; ◆ spatial bistability (stable F and M states); ● oscillatory M state. The empty symbols are attributed to the states of the CSTR: ▽ stable T state; △ stable F state; ◇ CSTR bistability (stable F and T states); ⊙ oscillatory state. The full and the dotted lines delineate the limit of the above different states of the OSFR and the CSTR respectively. (B, inset) Changes in the spatial bistability range as a function of w at $[BrO_3^-]_0 = 18$ mM.

Experimental Results

CSTR Dynamics. Let us first describe the observed CSTR dynamics of the BS reaction in the ($[NaBrO_3]_0$, $[H_2SO_4]_0$) plane (Figure 2). At low input concentrations of oxidant and acid, the CSTR contents are in the so-called "flow state" (F), characterized by a high redox potential and a high pH. In this F state, the extent of the reaction is low. When at fixed $[BrO_3^-]_0 = 18$ mM, the acid feed is increased stepwise, this F state remains stable in the range $[H_2SO_4]_0 = 0-12$ mM. Correlatively, in this range of acid feed, the pH decreases from 9.3 to 6.8. A further increase to $[H_2SO_4]_0 = 14$ mM leads the CSTR contents to switch to the so-called "thermodynamic state" (T), characterized by a low redox potential and pH. The T state is characterized by a high extent of the reaction, with a pH around 2.3. Upon decreasing stepwise the acid feed, this T state remains stable down to $[H_2SO_4]_0 = 5.6$ mM. A further decrease to $[H_2SO_4]_0 = 4.1$ mM makes the system switch back to the F state. The stability domains of these two steady-states thus overlap over a finite range of parameter values (see Figure 2). At $[BrO_3^-]_0 \leq 9$ mM the domain of bistability vanishes for

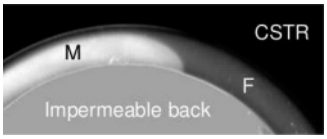

Figure 3. Illustration of an M/F state interface in the spatial bistability region with the M state propagating into the F state. In the annular part, dark and light gray areas correspond to low and high proton concentrations, respectively. Experimental conditions: $[BrO_3^-]_0 = 18$ mM, $[SO_3^{2-}]_0 = 60$ mM, $[H_2SO_4]_0 = 5.6$ mM, $w = 2.0$ mm.

$[H_2SO_4]_0 > 15$ mM. Beyond that, only continuous changes between a low and a high pH steady-state are observed.

At high concentration of the oxidant, a very narrow range of temporal oscillations can be observed between the monostable domains of the two previous steady-states (e.g., at $[BrO_3^-]_0 = 220$ mM large pH oscillations are observed for $[H_2SO_4]_0 = 1.9$ mM). Domains of temporal bistability and oscillation connect through a typical cross-shaped phase diagram topology.[17]

OSFR Dynamics. Let us now describe the chemical states of the annular OSFR when the CSTR contents belongs to the F state. The gel is fed with a mixture of the reactants at high pH and low extent of reaction. Only the color changes of the pH color indicator are monitored in the gel. At $[BrO_3^-]_0 = 18$ mM and $[H_2SO_4]_0 = 0$ mM, the gel is in a quasi-homogeneous dark state (high pH), also called the F state (Figure 3). When the acid feed is now increased stepwise, this F state of the gel remains stable up to $[H_2SO_4]_0 = 7.2$ mM. A further increase to $[H_2SO_4]_0 = 7.8$ mM makes the inner part of the annulus suddenly turn clear. A stable front, characterized by a color switch of the pH indicator, settles parallel to the rim of the annulus; this is the so-called mixed state (M) of the gel (Figure 3). By decreasing the $[H_2SO_4]_0$, the M state of the gel remains stable down to $[H_2SO_4]_0 = 5.6$ mM. At lower $[H_2SO_4]_0$, the F state is the only stable state of the gel. The stability range of the F and the M states of the gel overlap between $[H_2SO_4]_0 = 5.6$ and 7.2 mM, defining a spatial bistability domain. Within this range, one can create an interface between the F and M states, as illustrated in Figure 3. The relative stability of the two states naturally depends on the chemical feed values. It is now well-established that the extent of spatial bistability may sensitively depend also upon the width (w) of the OSFR.[11] In the present study, we have tested the sensitivity to this geometrical parameter by performing a few experiments at $w = 2$ mm. In these conditions, the range of spatial bistability, in the ($[H_2SO_4]_0$, w) plane, is shifted to slightly lower values of $[H_2SO_4]_0$ and becomes narrower (Figure 2).

At $[BrO_3^-]_0 = 150$ and 220 mM, there is no overlap between the steady-states of the gel. At these high values of the input concentration of the oxidant, increasing the $[H_2SO_4]_0$ from 0 mM, the F state of the gel becomes unstable at 1.1 and 0.8 mM, respectively. The inner part of the gel suddenly becomes acidic. As above, a front between a F (dark) and a T (clear) part forms, but this front is no longer stable and moves back and forth across the width of the gel (Figure 4). These spatiotemporal oscillations appear in a very narrow range of the parameters, as in the case of the CSTR (Figure 2). The overall topology of the OSFR phase diagram is similar to that of the CSTR.

Numerical Simulations

Our numerical simulations are based on the model of Szántó and Rábai[13] completed by the fast dissociation of HSO_4^- and water. The reactions steps, the reaction rates expressions, and the rate constants taken at 25 °C and used in the computations

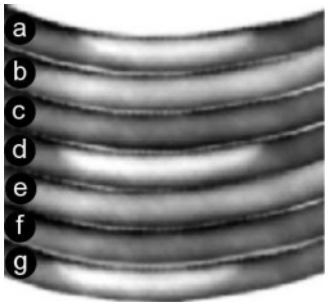

Figure 4. Spatiotemporal oscillations in the annular OSFR. Sequence of seven snapshots (a−g) taken at 25 min intervals. Feed and impermeable boundaries are located respectively at the bottom and top of each snapshot. Experimental conditions: $[BrO_3^-]_0 = 150$ mM, $[SO_3^{2-}]_0 = 60$ mM, $[H_2SO_4]_0 = 1.1$ mM, $w = 1.0$ mm.

are gathered in Table 1. The rate contants of the main processes are identical to those used in the original model report.[13] The rate constants corresponding to the protonation/deprotonation of weak acids were slightly modified to better fit well-established acid−base equilibrium values.

First, we computed the stable states in the CSTR for the experimental value of the residence time $\tau = 500$ s (i.e., a much shorter value than used in the original work of Szántó and Rábai). The computed phase diagram in the ($[H_2SO_4]_0$, $[BrO_3^-]_0$) phase plane is presented in Figure 5. The displayed dotted curves allow for an easy comparison with the experimental results. The two diagrams are in semiquantitative agreement, which is a remarkable result if one considers the simplicity of the model.

To compute the concentration profiles within the gel and the limits of the spatial bistability domains, we assume that, due to the small gel volume, the gel contents exert no feedback on the CSTR dynamics. Because H^+ and OH^- diffuse much faster than other ions, we have taken into account the effect of the ionic charges in the reaction−diffusion process. Accounting for the local electroneutrality within the gel, the reaction−diffusion equation for species i can be written as eq 1:[18]

$$\frac{\partial c_i}{\partial t} = R_i + D_i \nabla^2 c_i - \sum_j \frac{z_j}{z_i} (D_j - D_n) \nabla (t_i \nabla c_j) \qquad (1)$$

with

$$t_i = \frac{z_i^2 D_i c_i}{\sum_j z_j^2 D_j c_j}$$

where, for each species i, c_i is the concentration, R_i is the reaction rate term, D_i is the diffusion coefficient, z_i is the charge number, and t_i is the transference number. Species n is a reference species that is eliminated as a result of the electroneutrality condition. The Na^+ ion was taken as reference. It is a nonreacting species present as a counterion in the input feed. The charges and the values of the diffusion coefficients used in the computations are given in Table 2. The diffusion coefficients were taken from data in the literature,[18] when available. When they were not available, the values were fixed to arbitrary reasonable values and are marked by a star in the table. Note that the results should not significantly depend on these unknown values because the diffusivity of the corresponding species does not differ much from $D \sim 1 \times 10^{-5}$ cm^2 s^{-1}, which is the typical diffusion coefficient value of small species in aqueous solution. They have been adjusted to improve the fit with experimental observations. Also note that ionic species that are not implied explicitly in the rate laws of Table 1 (i.e., products)

TABLE 1: Kinetic Model Used in Numerical Simulations

reactions	rate laws	rate constants	ref
$BrO_3^- + 3HSO_3^- \rightarrow 3SO_4^{2-} + Br^- + 3H^+$	$r_1 = k_1[HSO_3^-][BrO_3^-]$	$k_1 = 0.0653\ M^{-1}\ s^{-1}$	13
$BrO_3^- + 3H_2SO_3 \rightarrow 3SO_4^{2-} + Br^- + 6H^+$	$r_2 = k_2[H_2SO_3][BrO_3^-]$	$k_2 = 18\ M^{-1}\ s^{-1}$	13
$BrO_3^- + 6H_2SO_3 \rightarrow 3S_2O_6^{2-} + Br^- + 6H^+ + 3H_2O$	$r_3 = k_3[H_2SO_3][BrO_3^-]$	$k_3 = 0.7\ M^{-1}\ s^{-1}$	13
$SO_3^{2-} + H^+ \leftrightarrow HSO_3^-$	$r_4 = k_4[SO_3^{2-}][H^+] - k_{-4}[HSO_3^-]$	$k_4 = 5 \times 10^{10}\ M^{-1}\ s^{-1}$; $k_{-4} = 3 \times 10^3\ s^{-1}$	12
$HSO_3^- + H^+ \leftrightarrow H_2SO_3$	$r_5 = k_5[HSO_3^-][H^+] - k_{-5}[H_2SO_3]$	$k_5 = 2 \times 10^8\ M^{-1}\ s^{-1}$; $k_{-5} = 3.4 \times 10^6\ s^{-1}$	12
$SO_4^{2-} + H^+ \leftrightarrow HSO_4^-$	$r_6 = k_6[SO_4^{2-}][H^+] - k_{-6}[HSO_4^-]$	$k_6 = 1 \times 10^{11}\ s^{-1}$; $k_{-6} = 1.148 \times 10^9\ M^{-1}\ s^{-1}$	6
$H^+ + OH^- \leftrightarrow H_2O$	$r_7 = k_7[H^+][OH^-] - K_w$	$k_7 = 1.4 \times 10^{11}\ M^{-1}\ s^{-1}$; $K_w = 10^{-14} \times k_7$	6

TABLE 2: Diffusion Coefficients[a]

species	z_i	$D_i \times 10^{-5}\ cm^2\ s^{-1}$
H^+	+1	9.312
BrO_3^-	−1	1.485
SO_3^{2-}	−2	1.1*
HSO_3^-	−1	1.5*
OH^-	−1	5.26
SO_4^{2-}	−2	1.065
HSO_4^-	−1	1.33
$S_2O_6^{2-}$	−2	1.0*
Br^-	−1	2.084
H_2SO_3	0	1.6*
Na^+	+1	1.334

[a] Asterisks correspond to our estimated values.

have been explicitly included in computations to ensure the balance of charges.

The computed domains of spatial bistability for $w = 1$ mm and $w = 2$ mm are reported in Figure 6. For convenience, the CSTR bistability limits are also displayed in the figure (dotted curves). As in experiments, the computed spatial bistability is restricted to a much narrower range of $[H_2SO_4]_0$ than for the CSTR bistability domain. This range decreases when the gel depth w increases. At large values of $[BrO_3^-]_0$, we always find a very narrow "pocket" of spatiotemporal oscillatory states (waves) within the gel at values for which the CSTR remains in the stationary F state. Results are in semiquantitative agreement with the experimental results in Figure 2.

Discussion

It is worth comparing our present observations on the BS reaction with those previously made with the homologous IS reaction. In both cases, the halate ions can be reduced all the way to halides, and the overall reactions are activated by protons. In CSTR conditions, both systems readily exhibit steady-state bistability between a high and a low pH state, over similar feed parameters and temperature ranges. The BS reaction can produce large amplitude pH temporal oscillations at very long residence times (i.e., above 1.8×10^3 s) and, as shown here, at very high bromate/sulfite feed ratios (i.e., $[BrO_3^-]_0/[SO_3^{2-}]_0 > 5$). This is more than 1 order of magnitude above the stoichiometric ratio of process R1. Such extreme conditions cannot be investigated in the case of the IS reaction. At feed concentrations on the order of 10^{-2}, diiodine precipitation occurs for iodate/sulfite ratios above 0.36, thus limiting the range of halate concentration over which the reaction system can be properly studied. Recent CSTR test experiments with the IS reaction showed no oscillatory behavior, even at residence times as long as 1×10^4 s, but only bistability.[19]

In an OSFR, both reaction systems exhibit "cross shape" phase diagrams where a domain of spatial bistability and a domain of large spatial oscillations of the acid−base front of a mixed state exchange at their "tips". However, in the IS system the oscillatory instability develops at low halate/sulfite ratios (i.e., < 0.32) and are connected to no obvious underlying CSTR oscillations, whereas in the BS system these are observed at high halate/sulfite ratios (i.e., > 1.7), and they closely follow, at slightly lower acid feed concentration, the domain of oscillatory dynamics in the CSTR. Careful explorations at the other end of the spatial bistability domain, at low halate/sulfite ratios, did not reveal any oscillatory dynamics. Only contin-

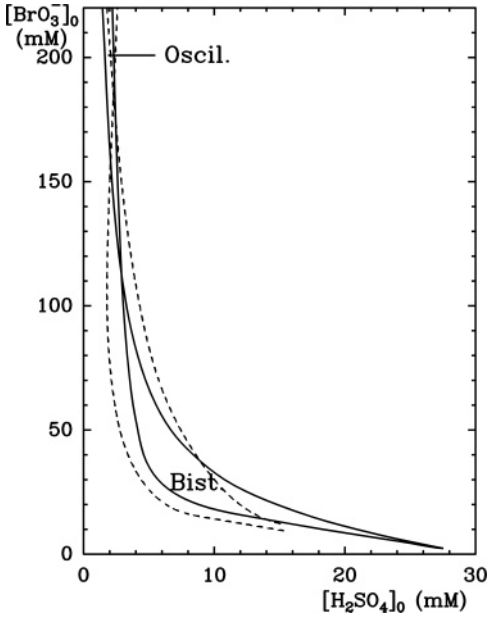

Figure 5. Nonequilibrium phase diagram in a CSTR. Solid lines: computed stability limits. Dotted lines: approximated experimental limits (from data in Figure 2). See text for conditions.

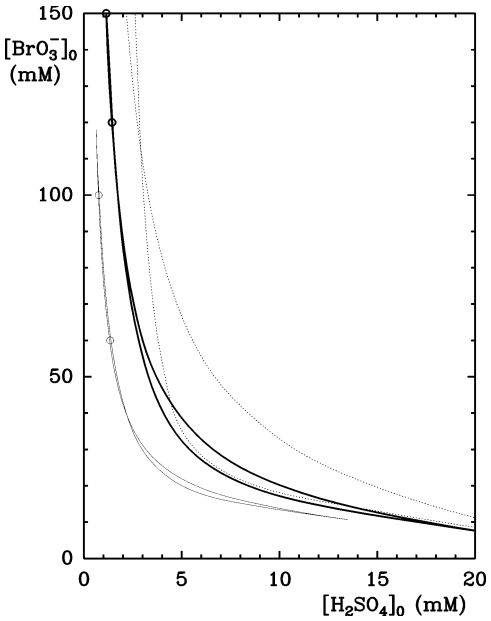

Figure 6. Computed spatial bistability domains in the OSFR. Heavy solid lines: stability limits of states for $w = 1$ mm; Light solid lines: stability limits of states for $w = 2$ mm; empty circles: values for which spatiotemporal oscillations were computed in the gel. Dotted lines: stability limits of the states of the CSTR (see Figure 5).

uous reversible changes in the OSFR steady-state were obtained as a function of feed parameters. The spatiotemporal oscillations observed with the BS reaction are essentially driven by the same kinetic instability that gives rise to homogeneous oscillations in a CSTR. Testing with numerical simulations of all species diffusing with a same diffusion coefficient of 1.5×10^{-5} cm ^{2} s^{-1} leads to spatiotemporal oscillations at similar contraint values of the phase diagram. Thus, the higher diffusivity of protons plays no fundamental role here.

In the mechanism proposed by Rábai and co-workers for the IS and BS reactions,[13,20] the authors assumed that the halogen species preferably react with sulfite rather than with each other. These models can account for a large set of batch and CSTR experimental observations.[20−22]

However, there is a significant difference between the mechanism of the IS and BS reactions. In the IS reaction, the dominant proton consuming process is the Dushman reaction (R3).[20]

$$IO_3^- + 5I^- + 6H^+ \rightarrow 3I_2 + 3H_2O \qquad \text{(R3)}$$

This process plays a major role with an excess of oxidant, especially at the end of the oxidation of the sulfite when the pH drops below 5. In batch experiments where $[IO_3^-]_0/[SO_3^{2-}]_0 \geq {}^1/_3$ (excess of iodate ions), the pH drops from 7 down to about 2.5, but then it can increase back to values up to 5.5, due to reaction R3. Furthermore, at the end of the sulfite consumption, the Dushman reaction with reaction R4

$$I_2 + HSO_3^- + H_2O \rightarrow 2I^- + SO_4^{2-} + 3H^+ \qquad \text{(R4)}$$

opens an additional iodide autocatalytic feedback loop that works in the same direction as the proton catalysis. The bromate−bromide reaction analogous to the Dushman reaction is too slow in the same pH interval (pH = 3−7) to be a significant proton scavenger, and no bromide autocatalytic path develops. To account for CSTR observations with the bromate−sulfite−ferrocyanide, Epstein et al.[12] developed kinetic models where the reactions between bromide and oxibromine species play a major role, but Rábai et al. showed that a kinetic model based on the direct reduction of oxibromine species by sulfite gives better fits[22] and is more consistent with previous meticulous kinetic studies[14,15] in the appropriate pH range. As a consequence, at high halate/sulfite ratios the M state of the BS reaction shows no pH rebound in the deepest part of the gel annulus after it has dropped, contrary to what is observed with the IS reaction.[7]

Remarkably, the spatial bistability domains of the two homologous reactions develop over very similar halate, sulfite, and sulfuric acid feed concentration ranges at the same temperature and residence time of the CSTR. This suggests that the overall sulfite reaction rates, and supposedly the redox mechanisms, are similar, at least as long as sulfite is present in a significant amount. We have shown that the skeleton mechanism in Table 1, based on the competition of the kinetic paths R1 and R2, leads to theoretical CSTR and OSFR phase diagrams in agreement with experimental observations. On the other hand, preliminary numerical calculations for the IS reaction based on a model that includes a kinetic path analogous to R1 together with R3 and R4 show that it can account for the CSTR and the OSFR bistability but not for the spatiotemporal oscillations at high acid feed and excess sulfite.[23] A one-electron-transfer kinetic path similar to R2 could be envisioned. Although the reduction potential of iodate ions (∼1.1 V) is lower than that of bromate ions (∼1.5 V), it is high enough for the formation of dithionate from sulfite (−0.57 V).[24] However, because no oscillations were observed at residence times even five times longer than for the BS reaction, the contribution of this kinetic path should be negligeable. In addition, such a kinetic path would a priori not favor oscillatory behavior at the low halate end of the spatial bistability domain. The origin of the spatiotemporal oscillations in the IS reaction still remains a challenge. On the contrary, the essential homogenuous and spatial dynamics of the BS reaction is very well understood and can be described in simple kinetic terms. This is a very promising system for further studies on reaction−diffusion and chemomechanical[25] patterns and would be an excellent model system to investigate chemically driven instabilities at fluid interfaces[26] in open reactors.

Acknowledgment. We thank the support of the Hungarian Research and Technology Innovation Fund and of the French−Hungarian Balaton program. Z. V. thanks the support from the ESA Topical Team. I.S. thanks the support of the Hungarian Scientific Research Fund (F049666, T0437473) and the Hungarian State Eötvös Fellowship. J.B. and P.D.K. are supported by CNRS and the French Agence Nationale de la Recherche.

References and Notes

(1) *Oscillations and Traveling Waves in Chemical Systems*; Field, R. J., Burger, M., Eds.; Wiley: New York, 1985.
(2) *Chemical Waves and Patterns*; Understanding Chemical Reactivity Kapral, R., Showalter, K., Eds.; Kluwer Academic Publisher: Dordrecht, 1995; Vol. 10.
(3) *An Introduction to Nonlinear Chemical Dynamics*; Epstein, I. R., Pojman, J., Eds.; Oxford University Press: New York, 1998.
(4) Borckmans, P.; Dewel, G.; De Wit, A.; Dulos, E.; Boissonade, J.; Gauffre, F.; De Kepper, P. *Int. J. Bifurcation Chaos Appl. Sci. Eng.* **2002**, *12*, 2307.
(5) Boissonade, J.; Dulos, E.; Gauffre, F.; Kuperman, M. N.; De Kepper, P. *Faraday Discuss.* **2001**, *120*, 353.
(6) Fuentes, M.; Kuperman, M. N.; Boissonade, J.; Dulos, E.; Gauffre, F.; De Kepper, P. *Phys. Rev. E* **2002**, *66*, 056205.
(7) Szalai, I.; De Kepper, P. *Phys. Chem. Chem. Phys*. **2006**, *8*, 1105.
(8) Murray, J. D. *Mathematical Biology*; Springer-Verlag: New-York, 1989.
(9) Szalai, I.; De Kepper, P. *J. Phys. Chem.* **2004**, *108*, 5315.
(10) Blanchedeau, P.; Boissonade, J. *Phys. Rev. Lett*. **1998**, *81*, 5007.
(11) Boissonade, J.; De Kepper, P.; Gauffre, F.; Szalai, I. *Chaos* **2006**, *16*, 037110.
(12) Edblom, E. C.; Luo, Y.; Orbán, M.; Epstein, I. R. *J. Phys. Chem.* **1989**, *93*, 2722.
(13) Szántó, T. G.; Rábai, G. *J. Phys. Chem. A* **2005**, *109*, 5398.
(14) Higginson, W. C. E.; Marshall, J. W. *J. Chem. Soc*. **1957**, 447.
(15) Williamson, F. S.; King, E. L. *J. Am. Chem. Soc.* **1957**, *79*, 5397.
(16) Labrot, V.; Hochedez, A.; Cluzeau, P.; De Kepper, P. *J. Phys. Chem.* **2006**, *110*, 14043.
(17) Boissonade, J.; De Kepper, P. *J. Phys. Chem*. **1980**, *84*, 501.
(18) Newman, J.; Thomas-Alyea, K. E. Chapter 11. *Electrochemical Systems*, 3rd ed.; Wiley: New York, 2004.
(19) Szalai, I. unpublished results.
(20) Rábai, G.; Kaminaga, A.; Hanazaki, I. *J. Phys. Chem. A* **1999**, *99*, 9795.
(21) Okazaki, N.; Rábai, G.; Hanazaki, I. *J. Phys. Chem.* **1995**, *103*, 10915.
(22) Rábai, G.; Kaminaga, A.; Hanazaki, I. *J. Phys. Chem.* **1996**, *100*, 16441.
(23) J. Boissonade, unpublished results.
(24) Latimer, W. M. *Oxidation Potentials*; Prentice Hall, Inc.: New-York, 1952.
(25) Labrot, V.; De Kepper, P.; Boissonade, J.; Szalai, I.; Gauffre, F. *J. Phys. Chem. B* **2005**, *109*, 21476.
(26) De Wit, A.; De Kepper, P.; Benyaich, K.; Dewel, G.; Borckmans, P. *Chem. Eng. Sci.* **2003**, *58*, 4823.